Collective dynamics of gastric cancer cells in fluid

Jiang Jiang,[1] Zhikun Zeng,[2] Zhaocheng Pan,[1] Bowen Shi,[1] Yujie Wang,[2,*] and Huan Zhang[1,†]
[1]*Department of Radiology, Ruijin Hospital, Shanghai Jiao Tong University School of Medicine, Shanghai 200025, China*
[2]*School of Physics and Astronomy, Shanghai Jiao Tong University, 800 Dong Chuan Road, Shanghai 200240, China*

(Received 8 July 2020; revised 24 September 2021; accepted 16 November 2021; published 2 December 2021)

Gastric cancer (GC) is the most common digestive system malignant cancer, and gastric cancer cells (GCC) can migrate in normal solid tissue and lymphatic fluid. Previously, much research has focused on the migration process when the cells are in the solid condition, such as migration through tissue, adhesion, and invasion processes, while little is known about the migration process of GCC in lymphatic fluid. In the current study, we investigate the migration of GCC in a fluid condition in an *in vitro* environment. We find that the cells diffuse mainly because of their cell viability. Therefore, despite the fact that lymph fluid is almost quiescent, GCCs can migrate around easily. The dynamics of cells also demonstrate a collective glassy dynamic similar to ordinary inactive glassy materials. As density of the cells increases, the movement of the cells becomes slower, and the collective dynamic becomes heterogeneous, which is similar to the dynamically heterogeneous behavior in glassy materials. The results will help us gain a better knowledge of the characteristics of GCC dynamics in the liquid phase which is crucial for the understanding of the mechanism for lymphatic metastasis. This can also potentially help early diagnosis of lymph node metastasis in GC and provide new insights for future clinical treatment.

DOI: 10.1103/PhysRevE.104.064402

I. INTRODUCTION

Gastric cancer (GC) is one of the most common malignant tumors of the digestive system worldwide, with approximately 950 000 new GC cases and 723 000 GC deaths every year [1,2]. GC has complex biological characteristics and is prone to lymph node (LN) metastasis at an early stage. Gotoda *et al.* found that the overall risk of LN metastasis in mucosal lesions was 2.7% and it could increase to 18.6% in submucosal lesions [3,4]. Once the LN metastasis occurs, the five-year survival rate would be less than 30% [5–7]. Therefore, detailed study of lymphatic metastasis of gastric cancer cells (GCC) is crucial for the prognosis of GC [3,4].

LN metastasis is a complicated process, which includes the GCC migration in both solid and fluid conditions [8]. It is found that the epithelial-to-mesenchymal transition (EMT) of malignant cells, by which cells transform their shapes to undergo a solidlike to liquidlike transition, would drive collective migration and eventually lead to metastasis [9,10]. Many studies have been conducted before to explore the migration dynamics and the solid-to-liquid transition at the cellular level in biological processes [11–16]. They found that behaviors of these processes, e.g., tumor metastasis, wound healing, and embryogenesis, are analogous to the glassy behaviors in atomic/molecular system, where the particle dynamics slow down significantly with the increase of the density or decrease of temperature. After drawing the analogy between cellular and physical systems, tools developed for investigating glass transition and glassy dynamics have been exploited to investigate the cell behaviors in biological systems, e.g., Angelini *et al.* [17] firstly illustrated that the cell relaxation dynamics slowed down as the cell density increased in Madin-Darby canine kidney layers. Later experimental study of Schötz *et al.* [14] also found evidence for cage effects, a hallmark behavior of glassy dynamics, in three-dimensional (3D) tissue explants from zebrafish embryos. Park *et al.* [18] experimentally studied the unjamming dynamics of bronchial epithelial cells by comparing cells from nonasthmatic donors and asthmatic patients. They first realized the relevance between cellular glassy dynamics and pathological diseases such as asthma. Following these experiments, Bi *et al.* [19] numerically simulated rheological behaviors of cells using the self-propelled Voronoi model, and have quantitatively explained the effects of cell cortical tension, adhesion, and motility on the collective cellular dynamics. Recently, studies have also been carried out to apply this model to investigate the metastasis of malignant tumor cells [8]. However, most studies have focused on the migration characteristics of malignant tumor cells in the solid condition [20–23], and little was known about their dynamics in the fluid condition. Since lymphatic fluid is the medium where GCC migrate to lymph node, it is therefore crucial to understand the migration dynamics of GCC in fluid condition. Naturally, it is reasonable to believe that great knowledge can be learned of the cellular dynamics in fluid condition by using the tools developed for studying dynamics of glass or jamming systems.

In the current study, we use a laser confocal microscope to investigate the GCC dynamics in fluid conditions to simulate the movement of GCC in lymphatic fluid. In such a system, there is only a weak adhesion force between cells, so that the GCCs tend to be spherical due to cortical tension. We find that the dynamics of GCCs demonstrate similar behaviors as that of glassy liquids, e.g., dynamical slowdown and dynamical heterogeneity, by increasing area fraction and weakening

*Corresponding author: yujiewang@sjtu.edu.cn
†huanzhangy@126.com

cells' own viability. The results help us gain a better knowledge of the feature of cellular dynamics in the liquid phase and provide new insights for future clinical treatment.

II. MATERIALS AND METHODS

A. Cell culture and transfection

AGS cell lines in this experiment were obtained from Ruijin Hospital, Shanghai Jiao Tong University and 293T cell lines were gifts from Professor L. Lv (Fudan University). AGS cells were cultured in Dulbecco's Modified Eagle Medium/Nutrient Mixture F-12 (DMEM/F12) supplemented with 10% fetal bovine serum and 1% penicillin-streptomycin at 37 °C in 5% CO2.

In order to acquire the 3D imaging of cells by the laser confocal microscopy, we need to transfect AGS cells by plasmids with green fluorescent protein gene. We used pCDHMSCV-MCS-EF1α-Green, PsPAX, and pMD2.G plasmids to complete the lentivirus packaging. After that, the AGS cells were transfected lentivirus with EZ trans according to the manufacturer's instructions. Finally, we cultured AGS cells with puromycin (2 μg/ml) for 2 weeks to stabilize the green fluorescence protein transfection.

To obtain a batch of low viability AGS cells (LVAC) as a control group of the normal AGS cells (NAC), different concentrations of cisplatin (0 μg/ml, 20 μg/ml, 30 μg/ml, 40 μg/ml and 50 μg/ml) were then added in the DMEM. After incubating the AGS cells with cisplatin for 2 h, the media was replaced with a completely fresh one and the cells were incubated for another 12 h. Cell Counting Kit-8 (CCK-8) was applied to initially evaluate the cell viability. Specifically, the absorbance value [O.D. (450 nm)] of the CCK-8 solution detected at 450 nm was measured by a microplate reader (Tecan Sunrise) after being incubated for 2 h.

B. Cell imaging

1. Fluorescence inverted microscopy

We photographed the green fluorescence protein positive (GFP^+) AGS cells with the fluorescence inverted microscope (EVOS M5000). We also compared the images taken through the bright field channel and GFP fluorescence channels (488 nm) [Figs. 1(a) and 1(b), respectively] to obtain the transfection efficiency. The number of cells observed in the bright field channel is the same with that in the GFP fluorescence channels. The results showed that the infection efficiency of the cells is 100%.

2. Laser scanning confocal microscopy (LSCM) imaging

We digested the cells with trypsin and imaged them in real time after resting the cell suspension for 20 min. A confocal microscope with ×300 objective was used to acquire images with a frame rate of 57 s per image over a 90 min period, and the field of view was 387.5 × 387.5 × 50 μm^3. Figure 2(a) shows the 3D reconstruction image obtained by laser scanning confocal microscopy.

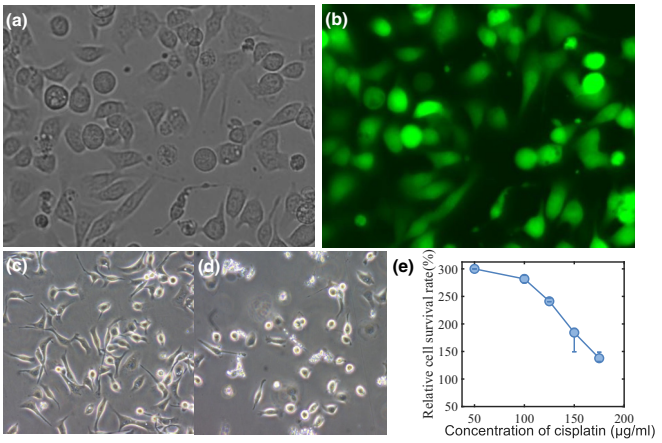

FIG. 1. Images by fluorescence inverted microscope of AGS cells through (a) bright field channel and (b) GFP fluorescence channel (488nm). Images of (c) normal AGS cells without cisplatin treatment and (d) the low viability AGS cells incubated with cisplatin (50 μg/ml) for 12 h. (e) The relative cell survival rate of AGS cells incubated with different concentration cisplatin for 12 h.

C. Image processing and tracking algorithm

To accurately determine the coordinates and volume of the cells, we used a marker-based watershed imaging segmentation technique to analyze the captured fluorescence 3D images [Figs. 2(c)–2(e)]. After converting the original image into a grayscale one, a serious problem we found is that the background illumination is nonuniform, and the fluorescence intensity varies from different cells. To tackle this issue, we performed a top-hat transformation to enhance the uniformity and used adaptive local thresholds to binarize the image. The standard "erosion" and "dilation" steps were carried out to remove the noise afterwards. After all these preprocessing steps, we can accurately segment the different cells by our

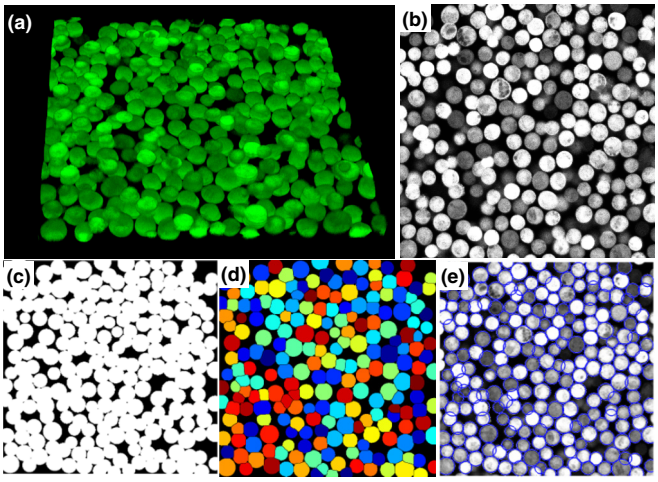

FIG. 2. (a) Three-dimensional reconstruction image of suspended cells by confocal microscope. (b) The 2D cross section with the maximum $\phi = 0.748$ of the 3D image stacks. (c) Binarized picture using adaptive local thresholds. (d) The color image of different cells segmented by a marker-based watershed algorithm. (e) The overlaid blue circles are cells optimized by a generalized Hough transform.

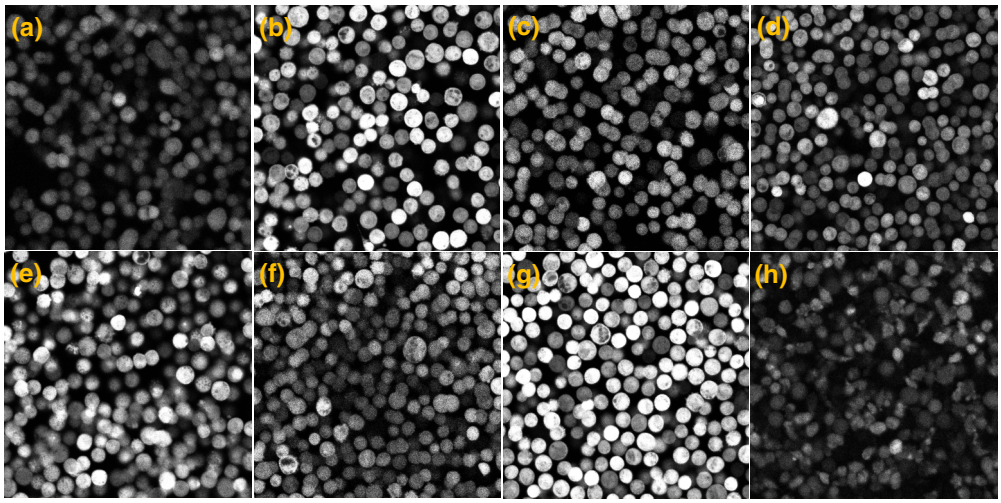

FIG. 3. The 2D cross section of the cell packing by confocal microscope of the NAC groups with $\phi =$ (a)0.527, (b) 0.596, (c) 0.634, (d) 0.675, (e) 0.715, and (f) 0.748, and (g) the MIXED group with $\phi = 0.672$.

in-house Matlab program based on watershed algorithm. In the end, we performed a generalized Hough transform to identify the individual cell as spherical particles for more accurate determination of cell centroids and radius, especially for those overlapping ones. Following this method, the 3D coordinates and sizes of more than 90% of the cells in the images could be obtained with an error less than 10^{-2} of the average cell diameter.

After the cells were segmented, the area fraction ϕ of the 2D cross-sections of the 3D image stacks could be calculated [Fig. 2(b)]. We calculated ϕ based on 2D Voronoi tessellation by using $\phi = \sum a_c / \sum a_{\text{voro}}$, where a_c and a_{voro} is the area and the Voronoi cell area of each cells respectively, and the sum is taken over all cells except ones closed to the boundaries which have incomplete Voronoi cells. The Voronoi tessellation was also implemented by an in-house Matlab program. Note that when there exists the ambiguity of cell overlap, we only calculated the overlapped area once. After calculating the area fractions ϕ of all cross-section slices, we selected the largest area fraction as the final ϕ of the current cell system.

Once we acquire the coordinates and sizes of the cells, their trajectories in the continuous shooting process could be obtained through a tracking algorithm: a cell in the first image is regarded as the same cell which is closest to it in the second image. Such a tracking algorithm works only if all the displacements between the same cells in two subsequent images are much less than the average intercell distance. In practice, the movement displacement of cells has to be less than half the cell diameter in two consecutive frames, which limits that our shooting time interval should be less than 1 min.

III. RESULTS

A. The viability of AGS cells

In order to compare the dynamics of normal AGS cells (NAC) and low viability AGS cells (LVAC), cisplatin was applied to treat the AGS cells (more details can be found in Sec. II). We performed CCK-8 assay to assess the viability of cells, which could be represented by the relative cell survival rate

$$S_{\text{rela}}(\%) = [(\text{O.D.}_{\chi\,\mu\text{g/ml}} - \text{O.D.}_{\text{blank}})/ (\text{O.D.}_{0\mu\text{g/ml}} - \text{O.D.}_{\text{blank}})] \times 100,$$

where χ is the concentration of cisplatin. With 50 μg/ml cisplatin, the relative cell survival rate decreased to 30% when the cells were incubated with cisplatin for 12 h, as shown in Fig. 1(e). We would use cells with this relative cell survival rate as a control group for experiments reported later. Nevertheless, AGS cells after treatment still maintained similar integral morphology as normal ones [Figs. 1(c) and 1(d)].

B. Area fraction of cells

Nine experiments were carried out in this work. The first to seventh experiments were conducted on cells of different densities without cisplatin incubation. In the eighth experiment, we used LVAC which had only 30% relative cell survival rate. In the ninth experiment, 50% NAC were mixed with 50% LVAC to explore the influence of cell viability on dynamics.

Before imaging, we used trypsin to digest the cells and rested the cell suspension for 20 min (it usually took 7-8 h for cells to sink to the bottom). Although the cells were in a 3D liquid environment before they settled to the bottom of the petri dish, the suspended cells were almost monolayers due to the similar settling speed [Fig. 2(a)]. It is therefore more suitable to use the area fraction ϕ to treat the system as a quasi-2D system instead of the volume fraction commonly used in a 3D system, even if our images were 3D.

Therefore, when calculating the area fraction ϕ, we chose from all the 2D cross sections of the 3D image stacks [Fig. 2(b)] and selected the layer with the largest area fraction as the final ϕ of the system (see Sec. II for more details).

The area fraction ϕ of the first to seventh experiments was 0.527, 0.596, 0.634, 0.675, 0.715, 0.720, and 0.748, respectively. The area fraction of the eighth experiment was 0.719,

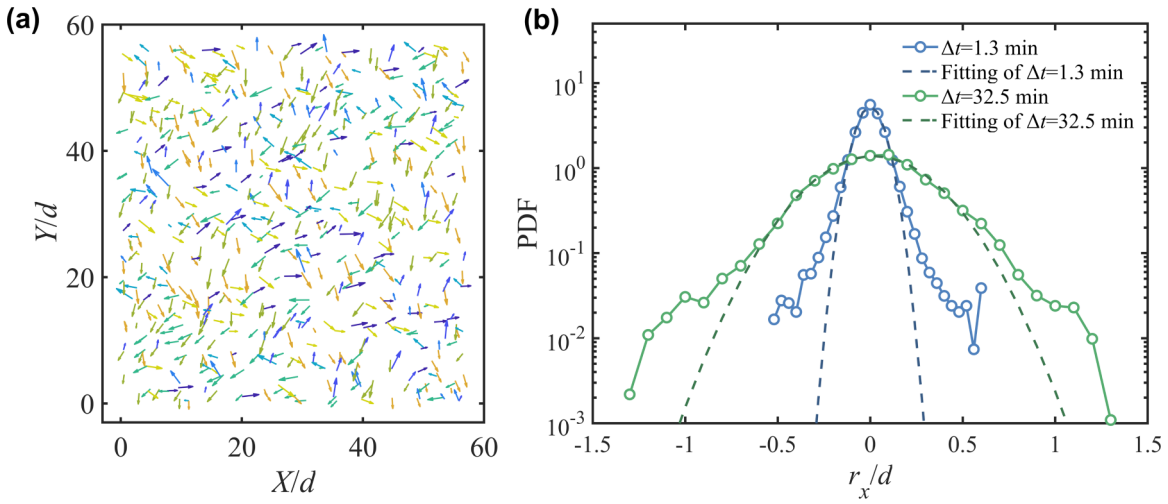

FIG. 4. (a) The displacement maps of GCCs of $\phi = 0.675$ within 20 min. The displacements of similar direction are marked by the same color. (b) The probability distribution of cell displacements in X direction of the fourth experiment with the area fraction $\phi = 0.675$ at time interval $\Delta t = 1.3$ and 32.5 min respectively.

almost the same as that of the fifth experiment, and that of ninth experiment was 0.672, almost the same as that of the fourth experiment. Figure 3 shows the 2D cross sections of the 3D image stacks at different cell densities.

C. Displacements maps, distributions and MSD

The displacement map of the AGS cells with $\phi = 0.675$ in a fluid environment was shown in Fig. 4(a). The results demonstrate that cells tend to move in random directions, which is unlike their behaviors in solidlike state, where cells tend to move as an integrity and show collective dynamics across long length scales.

However, the statistical analysis of cells displacements at different time intervals reveals that the movement of cells is not simply a diffusion behavior. As shown in Fig. 4(b), at short time scale, the probability distribution of AGS cell displacement $\Delta r = \mathbf{r}_i(t + \Delta t) - \mathbf{r}_i(t)$ is non-Gaussian, similar to those of glassy systems, while the distribution becomes more Gaussian-like at long timescale. This is related to the caging effect of the cells when their movements are confined by their neighbors at short timescales, suggesting dynamical heterogeneity.

MSD is conventional measure for microscopic dynamics, at time interval Δt:

$$\mathrm{MSD}(\Delta t) = \langle(\mathbf{r}_i(t + \Delta t) - \mathbf{r}_i(t))^2\rangle,$$

where $\mathbf{r}_i(t)$ is the location of cell i, $\langle \ldots \rangle$ means the average of different cells and of different starting time t. The self-diffusion coefficient $D = \lim_{\Delta t \to \infty} \mathrm{MSD}(\Delta t)/\Delta t$.

As shown in Fig. 5(a), the MSDs of cells moving along X, Y, and Z directions were calculated, and the corresponding self-diffusion coefficient D was obtained. It was found that MSD curves are very similar along X and Y directions, where D decreases with the increase of area fraction ϕ, as shown in Fig. 6(a). In the Z direction, the corresponding trend is less obvious due to the precipitation movement of the cells. The slope of MSD curve in the X direction approaches one in the long-time interval which suggests it becomes diffusive. D also decreases significantly when the cell viability decreases. This is clearly proven by a direct comparison of the MSDs of NAC and LVAC with similar ϕ, as shown in Fig. 5(b), and it was found that the diffusion of NAC was significantly faster than that of LVAC. This suggests that the movement of the cells in the experiment is mainly caused by their own viability. It is noted here that for the LVAC group, the slope of the MSD curve is greater than 1 on the long-time scale, as shown in Fig. 5(a). This is most likely due to the directional background flow which could not be completely subtracted and result in a cell drift, while this effect is less significant for the NACs.

D. Dynamics heterogeneity of GCCs in a liquid phase

The cells clearly exhibit glassy dynamics as area fraction increases. In order to quantify the structural relaxation in the system, the self-overlap order parameter Q was computed:

$$Q(\Delta t) = N^{-1} \sum_{i=1}^{N} \omega_i,$$

where N is the total number of cells. $\omega_i = 1$ if $|\mathbf{r}_i(t + \Delta t) - \mathbf{r}_i(t)| < 0.15d$ (d is the average diameter of GC) and $\omega_i = 0$ otherwise. Faster decay of the self-overlap order parameter suggests a smaller structural relaxation time. The overall trend is consistent with the MSD results, as shown in Fig. 5(c). In order to quantify potential collective cell dynamics in the system, we also calculated the four-point susceptibility χ_4 to characterize the dynamic heterogeneity in the system:

$$\chi_4 = N(\langle Q(\Delta t)^2\rangle - \langle Q(\Delta t)\rangle^2),$$

while $\langle \cdots \rangle$ denotes the temporal average. The peak time of χ_4 is roughly the structural relaxation time τ for ordinary glassy materials and the peak value of χ_4 quantifies the dynamic correlation length $\xi = (N_{\max}/\pi)^{1/2}$ and therefore the strength of the collective dynamics. Both peak time and height of the calculated χ_4 in the X direction increase with the increase of ϕ which suggests growing collective dynamics as

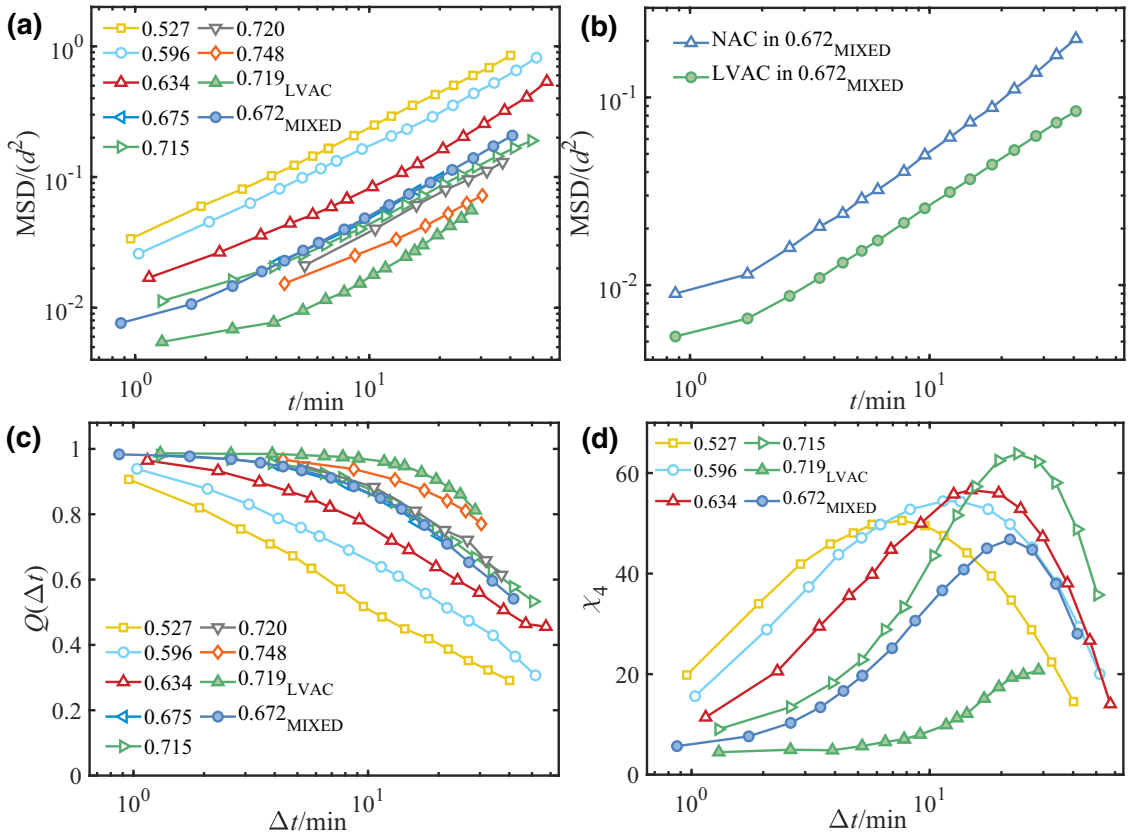

FIG. 5. Dynamics of GCCs. (a) MSD curves of GCCs for NAC groups whose area fraction $\phi = 0.527$, 0.596, 0.634, 0.675, 0.715, 0.720, and 0.748, LVAC and MIXED groups whose area fraction $\phi = 0.719$ and 0.672, respectively. (b) MSD curves for LVAC and NAC cells in the MIXED groups of $\phi = 0.672$. (c), (d) The auto-correlation overlap coefficient $Q(\Delta t)$ and the four point susceptibility χ_4 curves of GCCs as a function of time interval Δt.

ϕ increases [Fig. 5(d)]. According to the self-overlap order parameter Q, the structural relaxation time of the system is around $t = 20$ min, which is close to the peak time value of χ_4. It indicates the dynamic heterogeneity of the system reaches the maximum around structural relaxation time which is similar to ordinary glassy systems. As shown in Fig. 6(b), we use a power law to fit the dependency of relaxation time τ and dynamic correlation length ξ on area fraction ϕ by $\tau, \xi \sim 1/|\phi/\phi_0 - 1|^x$. Here, $\phi_0 = 0.84$ is the area fraction of maximum close-packing for 2D hard disks systems. The

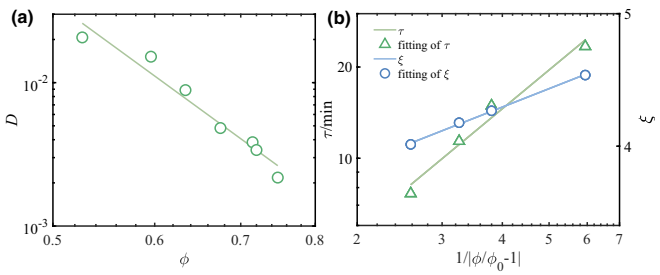

FIG. 6. (a) Self-diffusion coefficient D calculated by a linear fit of the MSD curves. (b) The corresponding time τ and length scales ξ associated with the collective dynamics as function of $1/|\phi/\phi_0 - 1|$. Lines are power-law fitting results.

obtained fitting exponents $x = 1.3$ for τ and $x = 0.14$ for ξ, while $x = 1.0$ for τ and $x = 1.7$ for ξ in air-driven 2D hard disk systems [24]. This means that the behaviors of the corresponding structural relaxation time and dynamic length scale of the system is not inconsistent with a divergence at ϕ_0 according to MCT prediction [24].

In our experiment, due to the lack of adhesion force between cells in a liquid phase, we can simply treat the cells as active Brownian particles. In related simulation work, Berthier *et al.* [25] found signatures of caging effects, as well as dynamically heterogeneous correlated motion for active systems, which was originally only observed in inactive glassy systems. This is consistent with the heterogeneous dynamics that we observed in the current work. Our work indicates that the heterogeneity of cells could also result from physical reasons while it has traditionally been solely attributed to biological origins. These results can therefore help future studies in understanding the heterogeneous behavior of cancer cells in realistic biological conditions. Likewise, we found that our cell system is easier to fluidize compared with the ordinary hard-disk inactive glass systems due to its viability, which is also reflected by the fact that the divergence of dynamic correlation length ξ with the increase of density is slower than that in the hard-disk system [24]. This reminds us that different from the simple glassy liquids, a lot of biological factors including cell-cell adhesion, cell mobility, and genetic

heterogeneities, should also be considered to understand the cellular collective migration and heterogeneity, as many studies suggested [9,10,12].

IV. CONCLUSION

Lymphatic fluid is the main medium for lymphatic metastasis. The clinical researches indicate that the metastasis can hardly be intervened once the GCCs invade into the lymph vessels. In this case, the five-year survival rate would be less than 30% [5]. Currently, much research explores the migration mechanisms in the solid phase, investigating its morphological, mechanical, and dynamical properties [8,26–28]. However, the migration characteristics in the fluid condition remain unknown. In this study, the dynamics of lymphatic metastasis of GCC in fluid condition is studied. We found that the motion of dense cells in a liquid phase is similar to that of a dense liquid approaching glass transition. With the increase of the cell density, the cell motions become slower. It forebodes the incipient glass/jamming transition when the dynamics of the system becomes stagnant. At the same time, we found that the system demonstrates collective dynamics also quite similar to ordinary glassy systems as evidenced by the non-Gaussian distribution of cell displacement distribution and increasing heterogeneous dynamics as area fraction increases [29,30]. The current study will complement existing experimental approaches when the system is already in a solid state by suggesting how the system can acquire rigidity from the liquid side. However, our cellular system also demonstrates unique active dynamics which are different from purely inactive particles and play critical roles in migration processes. Specifically, by decreasing the AGS cells viability to 30%, we found a significant decrease of the diffusion constant of the cancer cells, which suggests that the migration capability of the cells is greatly influenced by their viability instead of being simply driven by Brownian motion. Such a result is consistent with the results of previous simulation work. Clearly, the above results suggest that the cell dynamics can be slowed by either decreasing the cell's viability or increasing it density, which yields clues to potential clinic treatment methods. Additionally, as an integral part of the study of the GC lymphatic metastasis process, this study will help to establish a complete picture for lymphatic metastasis of GCC by shedding light on the nature of the migration process in the lymphatic fluid. This may potentially help early diagnosis of lymph node metastasis in GC and provide new insights for future clinical treatment.

ACKNOWLEDGMENTS

The work is supported by the National Natural Science Foundation of China (Grants No. 11974240 and No. 81771789), the Medical Engineering Cross Research Foundation of Shanghai Jiaotong University (Grants No. ZH2018QNA52 and No. YG2021QN08) and the Science and Technology Innovation Foundation of Shanghai Jiaotong University (Grant No. 21 X 010200829).

[1] R. L. Siegel, K. D. Miller, and A. Jemal, Cancer statistics, 2019, CA-Cancer J. Clin. **69**, 7 (2019).

[2] J. Ferlay, E. Steliarova-Foucher, J. Lortet-Tieulent, S. Rosso, J. W. W. Coebergh, H. Comber, D. Forman, and F. Bray, Cancer incidence and mortality patterns in Europe: Estimates for 40 countries in 2012, Eur. J. Cancer **49**, 1374 (2013).

[3] V. Pasechnikov, Gastric cancer: Prevention, screening and early diagnosis, World J. Gastroenterol. **20**, 13842 (2014).

[4] T. Gotoda, A. Yanagisawa, M. Sasako, H. Ono, Y. Nakanishi, T. Shimoda, and Y. Kato, Incidence of lymph node metastasis from early gastric cancer estimation with a large number of cases at two large centers, Gastric Cancer **3**, 219 (2000).

[5] M. M. Abdelfatah, M. Barakat, H. Lee, J. J. Kim, N. Uedo, I. Grimm, and M. O. Othman, The incidence of lymph node metastasis in early gastric cancer according to the expanded criteria in comparison with the absolute criteria of the Japanese Gastric Cancer Association: A systematic review of the literature and meta-analysis, Gastrointest. Endosc. **87**, 338 (2018).

[6] K. Yamashita, K. Hosoda, A. Ema, and M. Watanabe, Lymph node ratio as a novel and simple prognostic factor in advanced gastric cancer, Eur. J. Surg. Oncol. **42**, 1253 (2016).

[7] X. Zhang *et al.*, Endoscopic screening in asian countries is associated with reduced gastric cancer mortality: A meta-analysis and systematic review, Gastroenterology **155**, 347 (2018).

[8] L. Oswald, S. Grosser, D. M. Smith, and J. A. Käs, Jamming transitions in cancer, J. Phys. D **50**, 483001 (2017).

[9] P. G. Santamaria, G. Moreno-Bueno, F. Portillo, and A. Cano, EMT: Present and future in clinical oncology, Mol. Oncol. **11**, 718 (2017).

[10] J. P. Thiery, Epithelial-mesenchymal transitions in tumour progression, Nat. Rev. Cancer **2**, 442 (2002).

[11] A. Haeger, M. Krause, K. Wolf, and P. Friedl, Cell jamming: Collective invasion of mesenchymal tumor cells imposed by tissue confinement, Biochimica Et Biophysica Acta-General Subjects **1840**, 2386 (2014).

[12] A. Palamidessi *et al.*, Unjamming overcomes kinetic and proliferation arrest in terminally differentiated cells and promotes collective motility of carcinoma, Nat. Mater. **18**, 1252 (2019).

[13] J.-A. Park, L. Atia, J. A. Mitchel, J. J. Fredberg, and J. P. Butler, Collective migration and cell jamming in asthma, cancer and development, J. Cell Sci. **129**, 3375 (2016).

[14] E. M. Schotz, M. Lanio, J. A. Talbot, and M. L. Manning, Glassy dynamics in 3D embryonic tissues, J. R. Soc. Interface **10**, 20130726 (2013).

[15] K. D. Nnetu, M. Knorr, J. Käs, and M. Zink, The impact of jamming on boundaries of collectively moving weak-interacting cells, New J. Phys. **14**, 115012 (2012).

[16] S. Garcia, E. Hannezo, J. Elgeti, J.-F. Joanny, P. Silberzan, and N. S. Gov, Physics of active jamming during collective cellular motion in a monolayer, Proc. Natl. Acad. Sci. **112**, 15314 (2015).

[17] T. E. Angelini, E. Hannezo, X. Trepat, M. Marquez, J. J. Fredberg, and D. A. Weitz, Glass-like dynamics of collective cell migration, Proc. Natl. Acad. Sci. USA **108**, 4714 (2011).

[18] J. A. Park *et al.*, Unjamming and cell shape in the asthmatic airway epithelium, Nat. Mater. **14**, 1040 (2015).

[19] D. Bi, X. Yang, M. C. Marchetti, and M. L. Manning, Motility-Driven Glass and Jamming Transitions in Biological Tissues, Phys. Rev. X **6**, 021011 (2015).

[20] C. D. Paul, P. Mistriotis, and K. Konstantopoulos, Cancer cell motility: Lessons from migration in confined spaces, Nat. Rev. Cancer **17**, 131 (2017).

[21] P. Friedel, Y. Hegerfeldt, and M. Tusch, Collective cell migration in morphogenesis and cancer, Int. J. Dev. Biol. **48**, 441 (2004).

[22] J. A. Joyce and J. W. Pollard, Microenvironmental regulation of metastasis, Nat. Rev. Cancer **9**, 239 (2009).

[23] P. Friedl, Prespecification and plasticity: Shifting mechanisms of cell migration, Curr. Opin. Cell. Biol. **16**, 14 (2004).

[24] A. S. Keys, A. R. Abate, S. C. Glotzer, and D. J. Durian, Measurement of growing dynamical length scales and prediction of the jamming transition in a granular material, Nat. Phys. **3**, 260 (2007).

[25] L. Berthier and J. Kurchan, Non-equilibrium glass transitions in driven and active matter, Nat. Phys. **9**, 310 (2013).

[26] O. Chepizhko, M. C. Lionetti, C. Malinverno, C. Giampietro, G. Scita, S. Zapperi, and C. A. M. La Porta, From jamming to collective cell migration through a boundary induced transition, Soft Matter **14**, 3774 (2018).

[27] A. Lorentzen *et al.*, Single cell polarity in liquid phase facilitates tumour metastasis, Nat. Commun. **9**, 887 (2018).

[28] I. Pajic-Lijakovic and M. Milivojevic, Jamming state transition and collective cell migration, J. Biol. Eng. **13**, 73 (2019).

[29] A. Gandalovičová, T. Vomastek, D. Rosel, and J. Brábek *et al.*, Cell polarity signaling in the plasticity of cancer cell invasiveness, Oncotarget **7**, 25022 (2016).

[30] E. Scarpa and R. Mayor, Collective cell migration in development, J. Cell. Biol. **212**, 143 (2016).